Disclosing mineralogical phases in medioeval iron nails by non-destructive neutron techniques

Daniela Di Martino[a*], Enrico Perelli Cippo[b], Irene Uda[c], Maria Pia Riccardi[c], Roberto Lorenzi[d], Antonella Scherillo[e], Manuel Morgano[f], Costanza Cucini[g], and Giuseppe Gorini[a]

[a]*Dip. Fisica "G. Occhialini", Università degli Studi di Milano-Bicocca, piazza della Scienza 3, 20126 Milan, Italy*

[b]*Istituto di Fisica del Plasma "P. Caldirola", Consiglio Nazionale delle Ricerche, via Cozzi, 20126 Milan, Italy*

[c]*Dip. di Scienza della Terra, Università degli Studi di Pavia, via Ferrata, Pavia, Italy*

[d]*Dip. Scienza dei Materiali, Università degli Studi di Milano-Bicocca, via Cozzi, 20126 Milan, Italy*

[e]*STFC, Rutherford Appleton Laboratory, ISIS Facility, Chilton, UK*

[f]*PSI, Paul Scherrer Institute, Villigen, Switzerland*

[g]*Metallogenesi s.a.s. Milan, Italy*

**Corresponding author: daniela.dimartino@unimib.it*

Abstract

There is not only one methodology for the study of mineralogical phases in archaeological samples. In this paper we discuss a strategy applied to ancient iron nail samples completely based on non-destructive analyses. The archaeological samples come from the archaeological site of Valle delle Forme (province of Brescia – Italy) and date back to the 1300-1400 AD. Neutron based techniques, like time-of-flight neutron diffraction and neutron tomography, have been used to determine the mineralogical composition and the structure of nails. An independent check for the assessment of the presence of different mineralogical phases was given by Raman spectroscopy. The combination of different non-destructive techniques has provided very useful information on their chemical composition, nature of the patina and corrosion features of the nails (also in the bulk of the samples).

TEXT

Introduction

Corrosion is a natural process, affecting any metal conservation: corrosion reactions are to be monitored and eventually controlled to prevent degradation of materials. In the case of iron based materials, a long term air or soil exposition induces several mechanisms of oxidation/reduction combined to diffusion, precipitation and dissolution of iron compounds, in connection also with the environment (Cl, C, Si, or other elements present in air, water or soil could be relevant in chemical alteration).

Considering iron archaeological artefacts, many studies were already devoted to the understanding of the corrosion mechanisms -see for example Neff et al (2005, 2006), and references therein. Most of the metallurgical studies on the subject were based on the analysis of sample cross sections with invasive methods, like metallography and scanning electron microscopy (SEM): this is a severe limitation for archaeological items, where non-destructive experiments should be preferred. We thus attempted a different strategy, starting from neutron experiments. Our goal was to demonstrate that even with less-invasive techniques a reasonable amount of details may be obtained on both the appearance and composition of iron-based artefacts. Despite the fact that destructive methods (like metallographic analyses) are unbeatable in terms of accuracy and amount of information provided, they cannot be always applied to archaeological findings.

Neutron-based techniques have been already used in the archaeometallurgical field, with the paramount advantage of non-destructiveness. For example, time-of-flight neutron diffraction (TOF-ND) analyses disclosed bronze-related crystallographic phases -e.g. for Etruscan bronze artefacts (Festa et al. 2008) and steel-related phases -e.g. in Japanese swords (Grazzi et al. 2011) also allowing their quantification in a non–invasive way. Neutron resonance capture analysis (NRCA) was successfully employed for the study of bulk elemental composition -for example in Etruscan bronzes (Postma et al. 2004). Also neutron tomography (NT) was used for the analysis of metal artefacts, mainly statues (Kardjilov et al. 2006).

The novelty of the present study is the combination of all the mentioned neutron-based, non-destructive techniques to infer information on the mineralogical phases within a set of nails, coming from the archaeological site of *Valle delle Forme* (Brescia, Northern Italy) and dating back to the 1300-1400 AD. Valle delle Forme, thanks to the ongoing excavations, has given back a smelting plant of iron minerals, a forge for elaboration of semi-finished products, but also an "archaic" blast-furnace, and it could represent the "missing link" testifying the evolution from the bloomer to the blast furnaces techniques in iron production in northern Italy (Cucini and Tizzoni 1999, Cucini 2008). Seven specimens have been made available for the present study, and namely three completed nails, two fragments from a broken nail, one semi-finished nail and one "bloom fragment" (i. e. a spongy-like mass of iron and waste elements from the forge). All these specimens present of course heavily corroded surfaces. Phases likely to be present will include: *goethite* (α-FeOOH), *wustite* (FeO), *hematite* (Fe_2O_3) and *magnetite* (Fe_3O_4). Goethite is the main component of what is commonly known as rust. Also some modification of the previous phases could be present or completely different ones, like for instance carbides or silicates and derivatives. All these phases are of interest for understanding the conservation status of the nails, their composition and indication on the technological and corrosion processes. Our methodology was focused on the use of non-destructive techniques. Thus, we performed a neutron based characterization concerning mineralogical phases, through a TOF-ND and NRCA study run at ISIS (UK). In addition, we combined this study with Raman measurements too, in order to assign different mineralogical phases to different regions of the nail samples. The measurements aimed at disclosing different structures in the vibrational spectra as possible valuable indicators of specific corroded phases, in order to provide a sort of calibration for the analysis of the neutron diffraction data collected. We have to say that the Raman technique, though being a powerful tool for analyses on artistic items, has a limited penetration for opaque samples. In the case of the nails, in order to access the bulk of the materials to allow a better comparison with neutron techniques, it was necessary to make a cross section of a single nail, without any further destructive analyses. The "non-invasivity" of the Raman technique was thus, in the present case, somehow relaxed respect to the standard meaning; however, the used cross sections have been preserved and they may be used for further analysis. In this sense, the samples were not "destructed". Finally, two nails were investigated by NT at PSI (CH), resulting in the mapping of the volume of the nails from which the phases rich in H distinctly appeared.

Beyond non-destructiveness, our methodology has the advantage to infer mineralogical phases within a wide volume of the samples. Indeed, neutron techniques are bulk analyses, while metallographic techniques are often limited to the surfaces of cross sections considered.

Materials and methods

Our set of samples was part of a wider group of samples from Valle delle Forme (see the complete list of the samples given in table 1). Typical nail sizes are about 8x1x1 cm^3, 10 g in mass, heads of irregular shape and square section. All samples present a heavily corroded surface: an example of nail samples is depicted in figure 1. We analysed in detail 6 nail samples out of the set of several items, and a bloom fragment and in particular, samples number 3, 7, 8, 9, 15 & 16 were studied by ND and NRCA; sample number 15 was analysed also by Raman spectroscopy; samples number 3 and 4 were measured by NT.

Though limited in number, the analysed samples are representative of the complete group of samples from the archeological site of Valle delle Forme since the majority of discovered finished products were studied

Neutron measurements

The TOF-ND experiments were run at the Italian Neutron Experimental Station (INES) of the ISIS spallation neutron source (UK); INES is equipped with a system of "jaws" (i. e. beam limiters) in order to shape and reduce the beam size and to select the gauge volume of interest in the sample even in the millimetric range (in our case, selection of different spots within the nails was possible, and namely tip, body and head of each nail, see figure 1). The measurements were conducted in air, and the alignment was made through a laser pointer. The ND data were processed using the Mantid software (Arnold et al. 2014), for data normalization and correction, and then were analysed with the Rietveld refinement technique using the GSAS (General Structure Analysis System) code (Larson, Von Dreele 2004) with the EXPGUI interface (Toby 2001). By this procedure, the weight percentage of the identified phases can be quantitatively determined. In our Rietveld refinement, the TOF peak profile n. 3 has been used. Other refinements for all phases concern: background (function type 1), ZERO, DIFA and DIFC (TOF d-spacing conversion parameters), lattice parameters, phase concentration and profile parameters (sigma1, sigma2 and gamma1).
INES is a neutron diffractometer that offers the possibility of simultaneously performing ND and NRCA measurements (Imberti et al. 2008). The results in this case were only semi-quantitative. NRCA spectra were recorded detecting resonance peaks occurring in cross sections of neutron-induced capture reactions as a function of neutron energy. These peaks can be used to identify elements in materials. Details on the NRCA technique can be found for instance in the literature (Postma et al. 2001, 2007). Here we just mention that in NRCA energies of adsorbed neutrons are identified through the TOF technique; this means that the NRCA detector (in this case a YAP scintillator) records the arrival time of neutrons into the sample. The resulting spectra are thus shown as a function of time (see figure 2).
NT measurements were performed at the ICON beamline of the Swiss Spallation Neutron Source at PSI (CH). The ICON station is often devoted to archaeometric analyses (Lehmann 2006; Mannes et al. 2014) through the technique of neutron imaging. In this case, the so-called "midi-setup" was used together with a 5.5 Mpixels ANDOR-NEO camera with a pixel size, when focused on the scintillator screen, of about 50 μm. The exposure time for the white beam tomography was set at 15 s to profit from the full 16-bit dynamic range under ICON conditions. To save time, two nails were placed in the beam at the same time, rotating in parallel along the tomography central axis. In this configuration, the nails take turn to shadow each other, but the transmission along the line of highest thickness was measured to be in excess of 10%, mitigating the concerns of starvation artefacts. 1162 projections over 360 degrees were taken over the course of almost 5 hours of total exposure. Five dark currents and five open beam images were also taken for the correction of the images. The projections were then reconstructed into slices with the Octopus code (Dierick et al. 2004). To show the aspect of such images (both projections and slices), two videos were then mounted through image sequence with the ImageJ package.

Raman spectroscopy

Micro-Raman measurements were carried out at room temperature on cross sections of sample 15 by a confocal LABRAM (Jobin-Yvon) spectrometer, operating in backscattering configuration (with a focal layer thickness of few microns). A helium–neon laser (wavelength 632.8 nm, nominal power 17 mW) was used as exciting source with spectral resolution of about 2 cm^{-1}. The scattered light was detected by a CCD (SpectrumOne, Jobin Yvon). A microscope (Olympus BX40) was used to focus the excitation on the samples and to collect the scattered radiation, by three different objectives 20x/numerical aperture (NA) = 0.40, 50x/NA = 0.75 and 100x/NA = 0.95, with a resulting

sampled area of ~10, 5 and 2 μm in diameter, respectively. The sampled area could be selected after inspection of the sample surface, enlightened by an optical fiber, by a tele-camera. Each Raman spectrum is presented *as-recorded* using (unless otherwise stated) a 50x objective, and an integration time of 10 s. We note that no special preparation or treatment was required prior to micro-Raman measurements. However, only one sample was analysed by Raman measurements, since we avoided cutting (into cross sections) other samples. Direct measurements of laser power at the sample was recorded by a power meter, resulting in 1.0 mW, lower than the values reported for laser-induced thermal effects on iron oxides (Shebanova, Lazor 2003).

Results and discussion

Samples 3, 7, 8, 9, 15 and 16 were studied by ND and NRCA, selecting, whenever possible, different samples regions (see figure 1). Attribution of all peaks was made in agreement with data listed in table 2. As a result, the elements detected in our samples are displayed in table 3. In all the samples, NRCA spectra showed the expected, typical double peak from iron, while heads of sample 3 and 15 also presented two small peaks attributed to copper. The latter was also present in the spectra from the bloom fragment (sample number 16). Figure 2 shows a comparison of NRCA spectra of the bloom fragment (in black) and of the head of sample 15 (in red), displaying the peaks of iron and copper. Detection limits (and thus sensitivity) is strictly related to the elements considered. Our NRCA results are qualitative, but a relative estimate could be derived taking into account the area of the peaks and the relevant neutron cross sections. In particular Cu results in about 3 wt% in the bloom fragment and about 1wt% in the heads of sample 3 and 15, while As results in about 4 wt% in the bloom fragment.

ND patterns were recorded for samples 3, 7, 8, 9, 15 and 16. Unfortunately ND spectrum of sample 8 was not clearly readable, maybe for a wrong setting of the jaws. ND data for sample 3, 7, 9 and 15 are very similar and are dominated by the ferrite (Fe) phase. All peaks were assigned in agreement with the literature and an example is displayed for the three areas inspected within sample 15 (see figure 3). Data are shown as collected, without any smoothing procedure. All minor peaks are labelled: we could easily detect phases like magnetite, goethite, wustite and hematite, plus some cementite. Due to the presence of many overlapping peaks, and to the signal to noise ratio, an unambiguous attribution of all the co-existing phases is difficult. However, we applied a quantitative phase analysis with GSAS (see details given before).

The quantitative results are reported in table 4. We reported all phases clearly visible in the diffractograms. Though calculated detection limit (also depending on the phase) is generally reported at 0.1 wt% (see for example Grazzi et al. 2011), when concentration reached values below 0.5 wt% we preferred to indicate “traces”. The main iron oxides turn out to be magnetite or wustite, while goethite and hematite are present in less percentages (sometime trace phases). Other minor/trace phases are oxides and carbides. A very low weight percentage of Cementite (Fe_3C) has been detected. Since no other metal phases were present, the carbon content was derived by the formula:

$C[wt\%]=6.67 \bullet Fe_3C[wt\%]/(Fe[wt\%]+Fe_3C[wt\%])$ (see Fedrigo et al. 2015)

Concerning Cu, detected both in the nail heads and in the bloom fragment by NRCA, it could originate by some copper impurities already present in the starting material. Yet, we did not find any Cu-related phase in our neutron diffractograms of nails. Again, this could be related to the detection limit or to the absence of a crystalline structure (that is the copper compound could be in an amorphous phase).

Finally some silicates (like olivine, such as fayalite phases) are very likely, due to the presence of a band at d-spacing 4.25 Å, but in very small amounts (low percentages of amorphous phases could not be exactly quantified in our present GSAS analysis).

However, ND results could thus give reliable information on the main and minor mineralogical phases within the nail samples, in large area of samples and the following comments can be outlined concerning several mineralogical phases.

In all samples the main component is ferrite, which is the stable iron phase at room temperature.

Wustite (FeO) was detected in the bloom fragment (in agreement with the expected refining process) and only in traces in the nails (suggesting a good quality of the smelting process). In fact, wustite is a result of incomplete reduction, so it can be found in the bloom fragment, but not in finished iron products.

Other iron oxides, like magnetite and hematite, could be index both of the quality of refinement processes and conservation status.

Iron hydroxides, like goethite (FeOOH), are rust components and simply relates to the overall conditions of the artefacts. Only goethite was detected, but we cannot exclude the presence of other iron hydroxides beyond the detection limit, but also at higher concentration if in amorphous phase.

As far as carbon, whose quantitative determination is in relationship with the carburization level of the samples, we could give only an estimate, being cementite (Fe_3C) detected at about 0.5 wt%. In finished products studied C amounts are about 0.03-0.04wt%, as a mean, suggesting wrought iron artefacts.

Finally, Cu and As detection by NRCA, could not be related to crystalline phases, since ND data did not revealed any Cu- or As-bearing phase. These elements could be considered impurities in the starting ore minerals or in the materials used in the process technology. Moreover, the absence of any copper signal from the body and the tip of the nails could perhaps be related to the production technology (refinement of the iron alloy through hammering or other post-fusion processing).

The absence of troilite (FeS) could suggest smelting temperatures below 1000°C, since FeS forms at high temperatures.

The main limitation of ND is the spatial resolution. In fact, ND is a bulk technique (the neutrons cross the whole thickness of the samples) and the information about the presence of phases is integrated on the whole volume crossed by neutrons (an advantage with respect to surface or point analysis). On the other hand, the beam size (defining such volume) cannot be reasonably reduced below the millimetric scale because of flux considerations. In the present case, such volume intervals ("voxels") are thick as the whole sample, at least in the radial directions (see indicative representation of voxels in figure 1). This means that the phases present into a specific section of the nails are detected with no information about the depth from the artefact surface where they lie. As a result, we still lack the information about where phases different from ferrite are located in the inner/bulk part of the samples. This was derived by the Raman spectroscopy study only. One of the samples was indeed cross-sectioned, and examined through Raman spectroscopy. Spot measurements were performed along the sample, while a virtual section of the head of the nail was mapped. The mapping results are shown in figure 4.

The attribution of features in the Raman spectra was done in agreement with the literature (Neff et al. 2005, 2006; Bouchar et al. 2013), with the following criteria: i) peaks at 290 cm^{-1} and 390 cm^{-1} are assigned to goethite phase; ii) the band at 650 cm^{-1} is related to wustite phase; iii) hematite phase is associated with peaks at 220 cm^{-1} and 290 cm^{-1}; iv) the band at 670 cm^{-1} is attributed to magnetite phase; v) peak at 250 cm^{-1} is assigned to lepidocrocite. In particular, this phase is still an iron oxyhydroxide, defined by the chemical formula γ-FeOOH. Spot measurements in some of the inclusions detected within the metal phase disclosed calcite (with peak at 1088 cm^{-1}) and olivine (structured peak at 800 cm^{-1}) compounds.

Though the separation of the phases is not clearly defined, we could roughly identify several different layers, and namely:

- the external layer corresponds to a goethite (or lepidocrocite) phase, followed by a magnetite one (plus some wustite too);
- towards the bulk of the sample a hematite phase is detected;
- in the inner part of the sample, metallic phases are relevant and almost no Raman signal is detected. Only when inclusions occur, some peculiar Raman signals are evident.

Since the laser spot was 5 micron, the Raman results could give indications in the micron-scale region. Indeed, dimension of the different layers is always of the order of 50 to 100 microns. This information can be derived also by images collected through the optical microscope.

Raman results are in good agreement with ND data. Only lepidocrocite phase was not detected in ND patterns, so being probably a minor phase. Moreover, cementite and ferrite phases cannot be clearly recorded by Raman spectroscopy, but need other techniques (like ND) to be quantified. In particular, apart from sensitivity and other limitations, the nature of the two techniques is very different: bulky-like results are obtained by ND while Raman is typically point-like.

We would stress that Raman results provided an independent assessment for the presence of corrosion phases within nail number 15, at a micron size scale.

Finally, a neutron tomography study was conducted on samples number 3 and 4. An example of the recorded images is depicted in figure 5 along with two slices obtained through the tomography reconstruction process. In the case of radiographs, where the whole length of the nails is visible dark regions are the ones more interacting with neutrons, while the opposite occurs in the slices.

One tenth of the radiographs collected was used to make a movie, in order to clearly return the images of the whole nails, in different orientations (see video n.1). Moreover, after a reconstruction, also slices were obtained, and the corresponding movie was created (see video n.2). From both videos we could infer further details for the characterizations of the nails. We have to notice that in neutron radiography and tomography, the regions that appear to be more "intense" (i. e. darker in projections and lighter in slices) are known to be the richest in hydrogen in this case. Importantly, in the present samples, the only phase containing H is represented by goethite or lepidocrocite. Thus, FeOOH phases can be mapped along the whole volumes of the two nails analyzed, clearly returning the extension of the regions containing rust within the samples.

Samples 3 and 4 clearly exhibit some differences. First of all the shape of sample 3 appears irregular. This behaviour is evident also from an optical inspection, However, further details invisible at naked eye can be derived by radiographs, like for example an enhanced hydroxide phase presence above the fracture detected in the body of the nail number 3. This can be explained by a relevant penetration of atmospheric/soil agents (from the fracture) inducing enhanced corrosion mechanisms. Moreover, though sample 4 appears more regular in shape and less affected by rust, it is evident how at different virtual sections different rust penetration occurred, thus confirming that neutron radiographs can infer important indication on the conservation status. We stress that no other technique can derive the same information in a non-destructive way. Finally, thanks to our space resolution of about 50 μm, we could exclude the presence of H-bearing inclusion within the samples.

The use of neutron techniques, though not being new, is still a novelty in the study of cultural heritage artefacts and it should be carefully took into consideration when conservation and preservation issues of the samples are mandatory. Moreover, the samples can be analysed as they are, without any required preparation, so corrosion products and bulk of the sample could be inspected together. Obviously, the only limitation is the transportation: neutron measurements need to be performed in dedicated facilities and at the moment no on-site or mobile equipment is still available. Future studies could benefit also of ongoing developments of non-destructive neutron-based techniques, based on technological improvements, which will allow to reach higher resolutions and to perform several neutron analysis simultaneously.

Conclusions

In this paper, we have reported a new simple characterization procedure for the study of iron oxides in archaeological samples. We combined neutron-based and Raman analysis to a series of 600 years old nail samples. While these samples have not a museum importance, and could then in principle be the subject of destructive analysis, it is anyway worth to avoid as much as possible any kind of invasive analysis that can destroy the specimens: this is a general practice for every cultural heritage related sample. However, combining neutron and Raman analyses resulted in a twofold advantage. First of all, with Raman analysis performed on one sample, we could map the inner part of the nails

as a function of the mineralogical phases. It clearly appeared that a distribution of phases is present in this kind of samples, with the inner part of the nails richer in ferrite and other phases distributed along the radial direction. The same behavior can be clearly seen into the images of two un-sectioned nails examined through NT. Finally, the Raman mapping provided an independent input for a better interpretation of the neutron diffraction patterns from all the un-sectioned samples. With this approach, a whole series of related samples could be studied in a substantially non-invasive way, with the only sectioning of a single specimen among seven.

Importantly, the proposed strategy is directly applicable to characterization of many metals and ceramic objects, the only limitation being the access to neutron facilities. This approach may be of benefit in further nondestructive characterization in archaeometallurgy.

A further step will be exploiting energy resolved NT in order to map within a single NT different phases and not only H rich ones.

Acknowledgments

The authors wish to thank Giorgia Albani, for her assistance in TOF-ND measurements and Alberto Paleari for useful discussions on Raman measurements.

ISIS and PSI are gratefully acknowledged for the access granted to INES and ICON beamlines, respectively. In particular, the cooperation Agreement no. 06/20018 between CNR and STFC, concerning collaboration in scientific research at the spallation neutron source ISIS (UK), is gratefully acknowledged.

References

Arnold O et al. (2014) Mantid—Data analysis and visualization package for neutron scattering and μSR experiments. Nuclear Instruments and Methods in Physics Research Section A 764: 156-166

Bouchar M, Foy E, Neff D, Dillmann P (2013) The complex corrosion system of a medieval iron rebar from the Bourges' Cathedral. Characterization and reactivity studies. Corr. Sci. 76: 361-372

Cucini C, Tizzoni M (1999) La miniera perduta. Cinque anni di ricerche archeometallurgiche nel territorio di Bienno, Breno (La Valle delle Forme: i forni e le forge di epoca Bassomedievale, pp 201 – 214)

Cucini C (2008) Il maglio, la fucina, i forni e il pestaloppe della Valle delle Forme (Bienno, Brescia). Notizie Archeologiche Bergomensi 16: 227-248

Dierick M, Masschaele B, van Hoorebeke L (2004) Octopus, a fast and user-friendly tomographic reconstruction

package developed in LabView (R). Meas. Sci. Technol. 15: 1366–1370

Festa G, Caroppi PA, Filabozzi A, Andreani C, Arancio ML, Triolo R, Lo Celso F, Benfante V, Imberti S (2008) Composition and corrosion phases of Etruscan Bronzes from Villanovan Age. Meas. Sci. Technol. 19: 034004

Fedrigo A, Grazzi F, Williams A, Kabra S, Zoppi M (2015) J. Anal. At. Spectrom. 30: 707-712.

Grazzi F, Civita F, Williams A, Scherillo A, Barzagli E, Bartoli L, Edge D, Zoppi M (2011) Anal. Bioanal. Chem. 400:1493

ImageJ software: Image Processing and analysis in Java - http://imagej.nih.gov/ij/

Imberti S, Kockelmann W, Celli M, et al (2008) Measurement Science & Technology, 19: 034003

Kardjilov N et al. (2006) Neutron tomography for archaeological investigations. J. Neutron Res. 14: 29

Larson AC, Von Dreele RB (2004) General Structure Analysis System (GSAS), Los Alamos National Laboratory Report, LAUR pp 86-748

Lehmann E (2006) Scientific Reviews: Using Neutron Imaging Methods for Non-Invasive Investigation of Museum Objects. Neutron News 17: 22-29

Mannes D, Lehmann E, Masalles A, Schmidt-Ott K, Przychowski A, Schaeppi K, Schmid F, Peetermans S, Hunger K (2014) The study of cultural heritage relevant objects by means of neutron imaging techniques. Insight - Non-Destructive Testing and Condition Monitoring 56: 137-141.

Neff D, Dillmann P, Bellot-Gurlet L, Beranger G (2005) Corrosion of iron archaeological artefacts in soil: characterisation of the corrosion system. Corr. Sci. 47: 515-535

Neff D, Bellot-Gurlet L, Dillmann P, Reguer S, Legrand L (2006) Raman imaging of ancient rust scales on archaeological iron artefacts for long-term atmospheric corrosion mechanisms study. J. Raman Spectrosc. 37: 1228–1237

Octopus , a client server tomography reconstruction software, 2007 -http://www.xraylab.com

Postma H, Blaauw M, Bode P, Mutti P, Corvi F, Siegler P (2001) J. Radioanal. Nucl. Chem. 248: 115

Postma H, Schillebeeckx P, Halbertsma RB (2004) Neutron resonance capture analysis of some genuine and fake Etruscan copper alloy statuettes. Archaeometry 46: 635–46

Postma H, Perego RC, Schillebeeckx P, Siegler P, Borella A (2007) Neutron resonance capture analysis and

Applications. J. Radioanal. Nucl. Chem. 271: 95–9

Shebanova ON, Lazor P (2003) Raman study of magnetite (Fe3O4): laser-induced thermal effects and oxidation. J. Raman Spectrosc. 34: 845-852

Toby BH (2001) EXPGUI, a graphical user interface for GSAS, J. Appl. Cryst. 34: 210-213

TABLES

Table 1 Complete list of the samples from the archaeological site of Valle delle Forme (province of Brescia, Italy). The present study has been conducted on 6 nail samples and the bloom fragment.

N°	sample code	lenght (cm)	head width (cm)
1	US 6 (1997)	8	1.5
2	US 5b (1997)	8.5	2
3	US 111 (2006)	9	1.5
4	US 120 (2006)	10	2
5	US 1 (1997)	9.5	2
6	US 120	3	2
7	US 111 (2006)	5	1.5
8	US 111 (2006)	3	-
9	US 118E (2006)	4	-
10	US 108 (2006)	3.5	1.5
11	US 108 (2006)	-	1.5
12	US 116 (2006)	-	-
13	US 129 (2006)	5	2
14	US 127E (2006)	-	-
15	US Raman		
16	bloom fragment		

Table 2 List of main elements and relative peaks detectable by NRCA

Element	Peak1 (μs)	Peak2 (μs)	Peak3 (μs)	Peak4 (μs)	Peak5 (μs)
Fe	87	49	41		
Ag	724	409	299	230	
As	241	172	104	92	
Au	746	213	217	186	
Co	144	31	21		
Cr	41				

Cu	69	32	65		
Mn	89	50	41		
Mo	474	80	76	67	57
Ni	45	35	14		
P	10				
Pb	29	30	40	45	
S	9				
Sb	661	420	356	302	
Si	35	23			
Sn	265	156	87		
V	128	26			
W	815	375	356	602	
Zn	73	92	98	110	

Table 3 List of peaks detected by NRCA, and relative assignments, for samples 3, 7, 8, 9, 15 and 16.

Sample	**Peaks positions (μs) and relative assignments**
3 (tip)	48 (Fe), 88 (Fe)
3 (body)	48 (Fe), 88 (Fe)
3 (head)	32 (Cu), 40 (Fe), 48 (Fe), 68 (Cu), 88 (Fe)
7 (body)	48 (Fe), 88 (Fe)
7 (head)	48 (Fe), 88 (Fe)
8	48 (Fe), 88 (Fe)
9	48 (Fe), 88 (Fe)
15 (tip)	48 (Fe), 88 (Fe)
15 (body)	48 (Fe), 88 (Fe)
15 (head)	32 (Cu), 40 (Fe), 48 (Fe), 68 (Cu), 88 (Fe)
16	32 (Cu), 40 (Fe), 48 (Fe), 68 (Cu), 88 (Fe), 240 (As)

Table 4 Results of GSAS Rietveld analysis performed on the neutron diffractograms recorded on samples 3, 7, 9, 15 and 16. All data are in weight percentage (wt%). Phases in concentrations lower than 0.5% are considered traces.

Nail 3/part	**Ferrite**	**Magnetite**	**Goethite**	**Hematite**	**Wustite**	**Cementite**	**Fayalite**

head	99.2	0.5	traces	traces	traces	0.5	traces
body	92.7	7.1	traces	traces	traces	traces	traces
tip	87.7	12.0	traces	traces	traces	traces	traces
Nail 7/part	**Ferrite**	**Magnetite**	**Goethite**	**Hematite**	**Wustite**	**Cementite**	**Fayalite**
head	99.2	0.5	traces	traces	traces	traces	traces
body	97.2	2.6	traces	traces	traces	traces	traces
Sample 9	**Ferrite**	**Magnetite**	**Goethite**	**Hematite**	**Wustite**		
	86.5	12.0	traces	traces	1.4		
Nail 15/part	**Ferrite**	**Magnetite**	**Goethite**	**Hematite**	**Wustite**	**Cementite**	**Fayalite**
head	90.2	6.2	2.6	traces	traces	0.5	traces
body	93.1	7.2	traces	traces	traces	traces	traces
tip	90.8	8.9	traces	traces	traces	traces	traces

FIGURE CAPTIONS

Fig. 1 Picture of nails sample measured at INES (ISIS, UK): the red rectangles (not in scale) represent the voxels, i.e. the volumes inspected by neutron analysis, while the figures in black refer to sample numbers

Fig. 2 NRCA results for sample 15 (in red) and 16 (in black); iron and copper peaks are indicated by arrows

Fig. 3 ND data for sample 15, obtained from bank number 6 at INES diffractomer (ISIS, UK), in three different points of the nail: head (in red), body (in green) and tip (in black). Several mineralogical phases were detected. To enhance lower peaks, a semilog scale is used. Peaks were labelled in the following way: **F** corresponds to ferrite, **a** to magnetite and wustite, **b** to cementite and magnetite, **c** to cementite, hematite and goethite, **d** to cementite, **e** to cementite, **f** to wustite, **g** to cementite, **h** to cementite, **i** to wustite and cementite, **l** to magnetite, **m** to magnetite.

Fig. 4 Raman results: mapping of the head of nail sample 15. Upper part: reference spectra and spectra recorded in points A, B, C, D. Lower part: map of a virtual section of the head nail, with the distribution of phases. The map is the result of the ratio between peak and baseline signals, in the following regions: magnetite: peak: 665-680 cm^{-1}, baseline: 585-598 cm^{-1}; lepidocrocite: peak: 242-256 cm^{-1}, baseline: 287-272 cm^{-1}; hematite: peak: 215-233 cm^{-1}, baseline: 256-271 cm^{-1}; wustite: peak: 650-660 cm^{-1}, baseline: 581-598 cm^{-1}

Fig. 5 Example of a neutron tomograph on a couple of iron nails (left side); the reconstructed virtual sections (highlighted by a yellow arrow) are shown (right side)

Figures

Figure 1

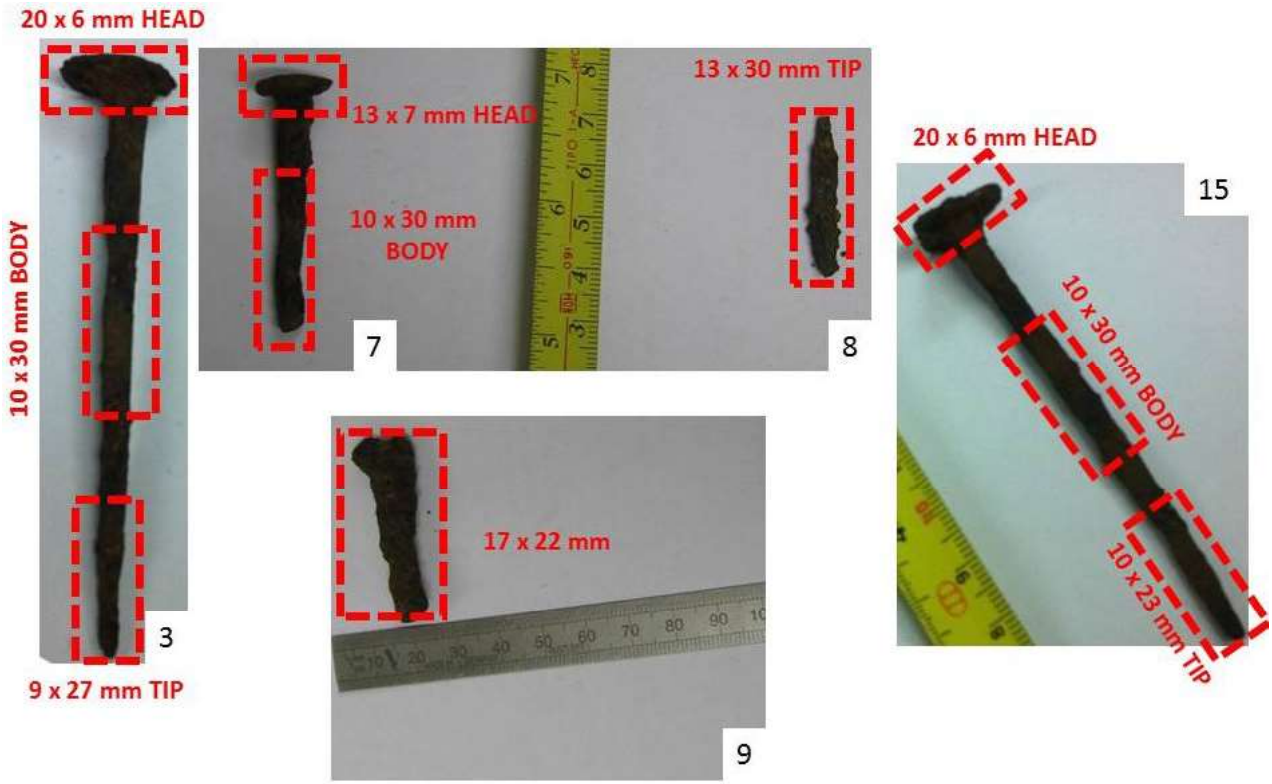

Figure 2

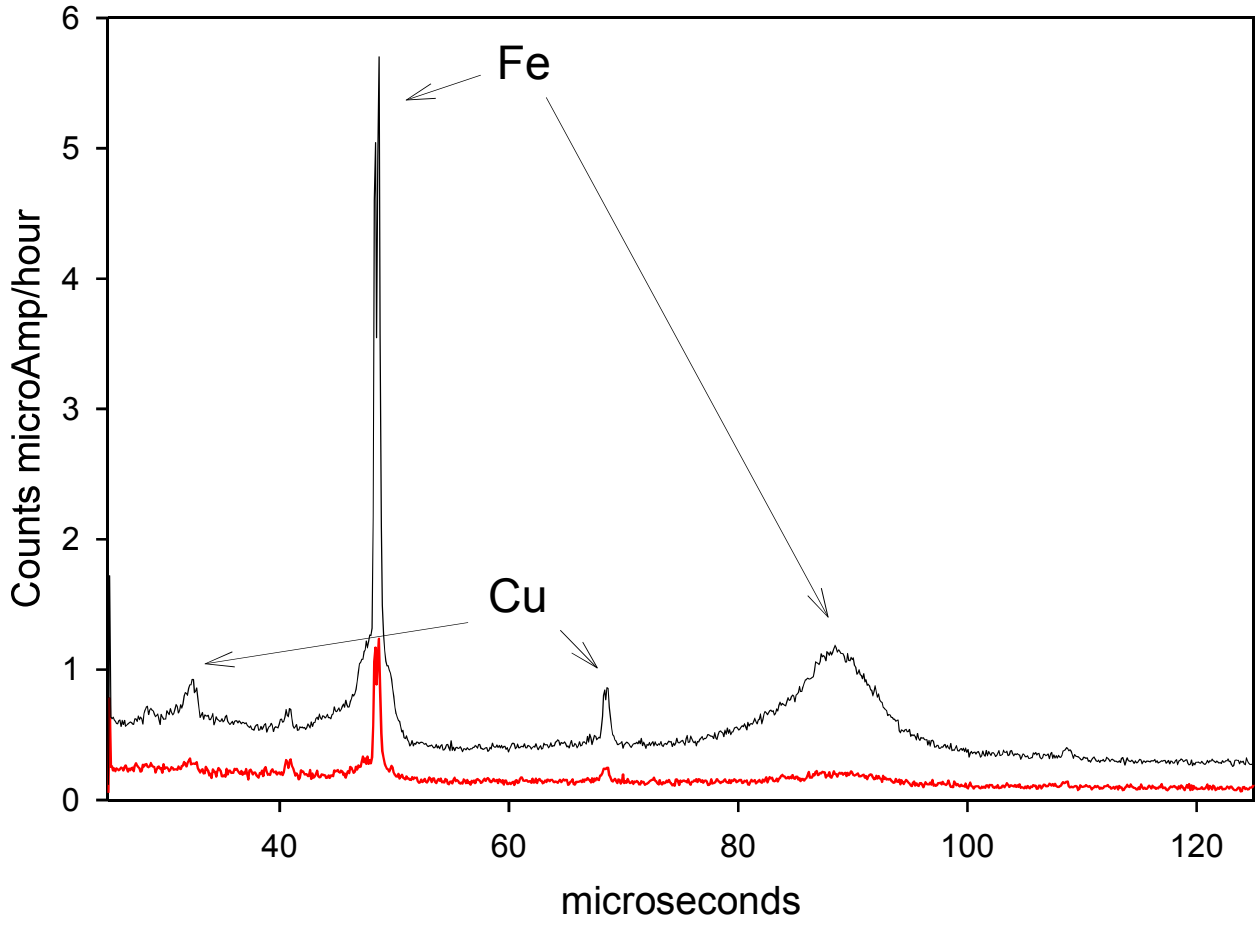
Fe
Cu
Counts microAmp/hour
microseconds
0
1
2
3
4
5
6
40
60
80
100
120

Figure 3

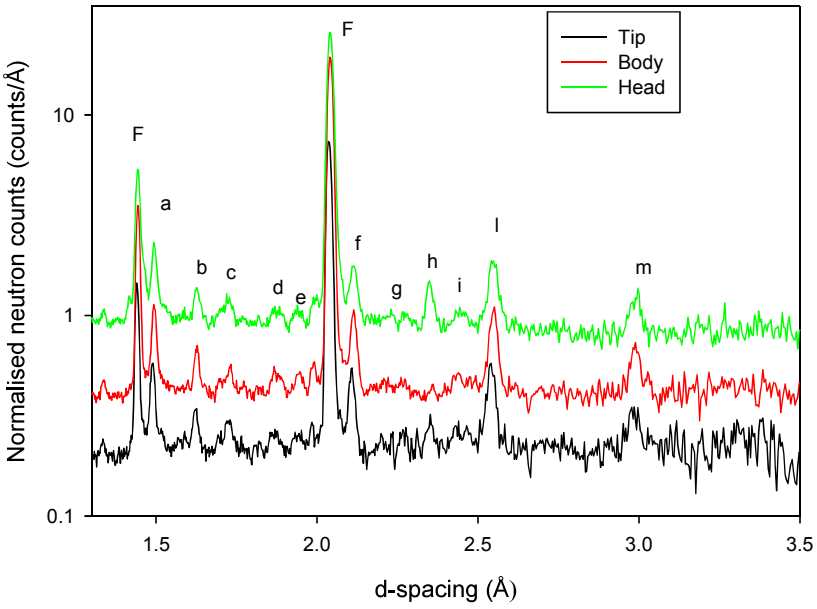
Tip
Body
Head
Normalised neutron counts (counts/Å)
d-spacing (Å)
10
1
0.1
1.5
2.0
2.5
3.0
3.5
F
a
b
c
d
e
F
f
g
h
i
l
m

Figure 4

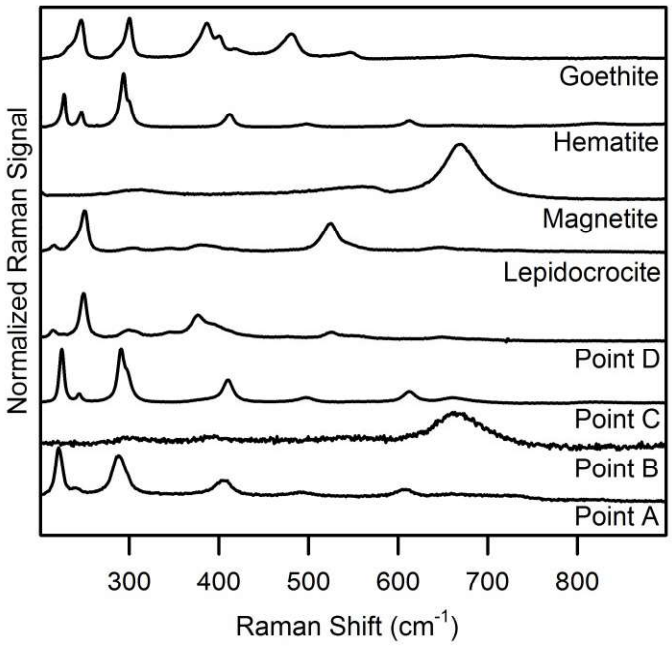
Goethite
Hematite
Magnetite
Lepidocrocite
Point D
Point C
Point B
Point A
Normalized Raman Signal
300
400
500
600
700
800
Raman Shift (cm-1)

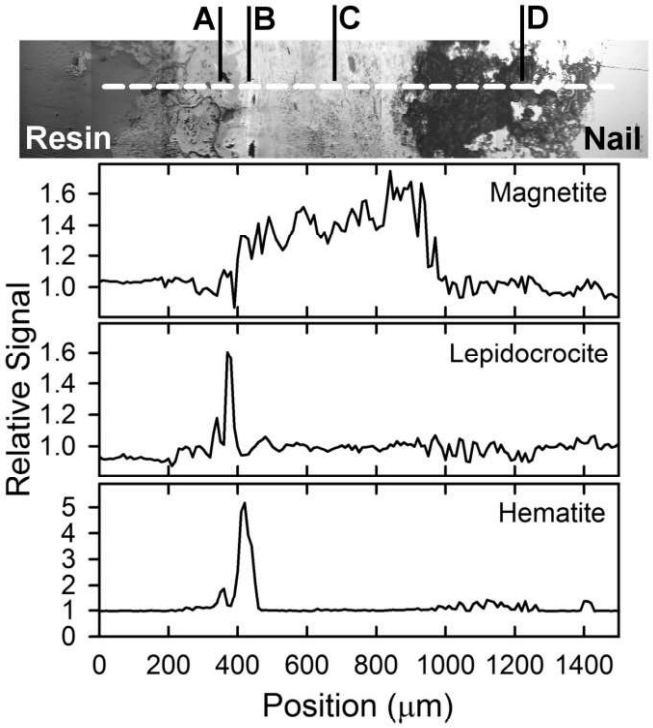
A
B
C
D
Resin
Nail
Magnetite
Lepidocrocite
Hematite
Relative Signal
1.0
1.2
1.4
1.6
0
1
2
3
4
5
0
200
400
600
800
1000
1200
1400
Position (μm)

Figure 5